Food and Chemical Toxicology 174 (2023) 113638

Contents lists available at ScienceDirect

Food and Chemical Toxicology

journal homepage: www.elsevier.com/locate/foodchemtox

Narirutin. A flavonoid found in citrus fruits modulates cell cycle phases and inhibits the proliferation of hormone-refractory prostate cancer cells by targeting hyaluronidase

Shilpi Singh [a,b], Akhilesh Kumar Maurya [c], Abha Meena [a,b,*], Nidhi Mishra [c], Suaib Luqman [a,b,**]

[a] Bioprospection and Product Development Division, CSIR-Central Institute of Medicinal and Aromatic Plants, Lucknow, 226015, Uttar Pradesh, India
[b] Academy of Scientific & Innovative Research (AcSIR), Ghaziabad, 201002, India
[c] Department of Applied Sciences, Indian Institute of Information Technology Allahabad, Prayagraj, Uttar Pradesh, India

ARTICLE INFO

Handling Editor: Dr. Bryan Delaney

Keywords:
Narirutin
Chemoprevention
Prostate cancer
Hyaluronidase
ROS

ABSTRACT

Narirutin is a dietary flavanone found in lemons, oranges, passion fruit, bergamot and grapefruit. It possesses anti-allergic, cardioprotective, neuroprotective, hepatoprotective potential, and its enriched fraction suppresses the growth of prostate cancer cells; however, there is currently no information on the chemopreventive potential of narirutin alone against hormone-refractory prostate cancer cells (PC-3) and its mode of action. Thus, the chemopreventive possibility of narirutin was investigated in PC-3 cells by utilising cytotoxicity assays. Further, a mechanism was deduced targeting hyaluronidase, an early-stage diagnosis marker, by cell-free, cell-based and *in silico* studies. The results indicate that narirutin reduced the viability of PC-3 cells with the inhibitory concentration range of 66.87–59.80 μM. It induced G0/G1 phase arrest with a fold change of 1.12. Besides, it increased the generation of reactive oxygen species (ROS) with a fold change of 1.34 at 100 μM. Narirutin inhibited hyaluronidase's activity in cell-free (11.17 μM) and cell-based assays (67.23 μM) and showed a strong binding interaction with hyaluronidase. Finally, the MD simulation analysis supported the idea that narirutin binding enhanced compactness and stability and created a stable complex with hyaluronidase. In addition, ADMET prediction indicates that it is a non-toxic, non-CYPs inhibitor and thus didn't alter the metabolism. The results reveal that narirutin may be a potential chemopreventive agent for hormone-resistant prostate cancer cells in addition to offering data for supporting diet-based nutraceutical agents to prevent prostate cancer.

1. Introduction

Prostate cancer is the most commonly diagnosed cancer associated with androgen receptors and prostate-specific antigens (Kallifatidis et al., 2016). After receiving androgen restriction therapy for advanced prostate cancer, the patient's tumors eventually developed into hormone-refractory prostate cancer (HRPC). The hormone-refractory tumor treatment is chemotherapy; however, improving the therapeutic efficacy without adverse effects on normal cells is the major challenge associated with HRPC treatment (Cheng et al., 2018; Rawla, 2019). The use of complementary and alternative medicine has increased in the past few decades as it boosts the immune system, reduces the chances of relapse, decreases the therapeutic side effects and supports conventional therapies. According to the reports, complementary and alternative medicine is used by 50% of prostate cancer patients, and among these compounds originating from plants are most frequently utilised (Bahall, 2017; Drozdoff et al., 2018; Zuniga et al., 2019; Toygar et al., 2020). The evidence indicates that targeting prostate cancer cells with nutraceuticals is the ideal strategy for HRPC prevention (Fontana et al., 2020). Narirutin is a flavanone glycoside commonly found in grapes and citrus fruits. It is the main component of various herbal formulations, including Xue fu Zhuyu Decoction, Simo decoction, Xiao-Cheng-Qi Tang, Hou-Po-San-Wu Tang, and Hou-Po-Da-Huang Tang decoction, Huoxiang Zhengqi oral liquid, Hyeonggaeyeongyotang decoction, Kampo Prescriptions, Five-citrus type crude drug, Qili Qiangxin capsule, Fructus Aurantii-type formulae, Wen-Dan Decoction (Chun-yan et al., 2020; Zhang and Cheng, 2006; Fu et al., 2016; He et al., 2018; Chen

* Corresponding author. Bioprospection and Product Development Division, CSIR-Central Institute of Medicinal and Aromatic Plants, Lucknow, 226015, Uttar Pradesh, India.
** Corresponding author. Bioprospection and Product Development Division, CSIR-Central Institute of Medicinal and Aromatic Plants, Lucknow-226015, Uttar Pradesh, India.
E-mail addresses: a.meena@cimap.res.in (A. Meena), s.luqman@cimap.res.in (S. Luqman).

https://doi.org/10.1016/j.fct.2023.113638
Received 27 December 2021; Received in revised form 18 January 2023; Accepted 24 January 2023
Available online 25 January 2023

Abbreviations

Ab/Am	Antibiotic/antimycotic
AhR	Aryl-hydrocarbon receptor
BACE-1	Beta-site amyloid precursor protein cleaving enzyme 1
BE	Binding energy; −2
DMEM	Dulbecco's minimal essential media
DMSO	Dimethyl sulfoxide
EMT	Epithelial-mesenchymal transitions
ERK	Extracellular signal-regulated kinase
FBS	Fetal bovine serum
FACS	Fluorescence-Activated Cell Sorting
GAPDH	Glyceraldehyde 3-phosphate dehydrogenase; HA, Hyaluronic acid
HEPES	N-2-hydroxyethylpiperazine-N′-2-ethanesulfonic acid
IC_{50}	Half maximal inhibitory concentration
HRPC	Hormone-refractory prostate cancer
HYAL	Hyaluronidase
IP-10	Interferon gamma-induced protein 10
MTT	3-(4,5-dimethylthiazol-2-yl)-2,5-diphenyltetrazolium bromide
NAC	N-acetyl L-Cysteine
NAR	Narirutin
NADPH	Nicotinamide adenine dinucleotide phosphate hydrogen
NRU	Neural red uptake
NaOH	Sodium hydroxide
NFκB	Nuclear factor kappa B
PDT	Podophyllotoxin
PI	Propidium iodide
PDB	Protein Data Bank
PCR	Polymerase chain reaction
PBS	Phosphate buffer saline
PPARβ	Peroxisome-proliferator-activated receptor β
RNase A	Ribonuclease A
RIPA	Radio immune precipitation assay buffer
ROS	Reactive oxygen species
SRB	Sulforhodamine B
TCA	Trichloroacetic acid

et al., 2015; Yu et al., 2013; Seo and Shin, 2020; Tsujimoto et al., 2019; He et al., 2020; Zhang et al., 2019). Narirutin did not affect the vitality of M1 macrophages, but it did decrease the lipopolysaccharide-induced interferon-gamma-inducible protein synthesis in THP-1-derived M1 macrophages. It reduced the IP-10 expression by modulating the aryl-hydrocarbon receptor (AhR), peroxisome-proliferator-activated receptor β (PPARβ), and α, estrogen receptor, and altered the histone acetylation in macrophages (Li et al., 2020). Employing Autodock-vina computational binding analysis, narirutin binds to the SARS-CoV-2 major protease with a binding affinity of -8.9 kcal/mol (Ngo et al., 2020). Another study found that narirutin has a binding affinity of -8.1 kcal/mol for the 3C-like protease of SARS-CoV-2. (Cherrak et al., 2020). Pre-treatment with narirutin reduces transfer latency by reducing neuronal swelling and cell membrane disruption (Patel et al., 2020). According to the molecular interaction study, narirutin suppresses BACE-1 activity by repelling water molecules. It decreases the aggregation of Aβ by up to 53% at 20 nM but inhibits BACE-1 activity by up to 79.3% at 500 nM. (Chakraborty and Basu, 2017). Besides, earlier findings and preliminary studies are insufficient to define its anti-proliferative property in hormone-refractory prostate carcinoma (PC-3) cells.

Hyaluronidase is involved in the degradation of hyaluronic acid into small fragments. A high level of hyaluronidase and hyaluronic acid has been reported in the tissues of prostate cancer patients (Lokeshwar et al., 2001). Compared to benign hyperplastic tissue and normal prostate tissues, prostate cancer cells secrete at least ten times more hyaluronidase, which is connected with metastasis and tumor grade. The over-expression of hyaluronidase promotes tumor growth, metastasis and angiogenesis (Lokeshwar et al., 1996; Josefsson et al., 2011). Overexpression of hyaluronidase and hyaluronic acid assisted in predicting the clinical recurrence of prostate cancer and decreased survival by five-year (Gomez et al., 2009). Hyaluronidase is reported as the novel biomarker involved in the pathophysiology and early diagnosis of prostate cancer (Skarmoutsos et al., 2018). Targeting hyaluronidase may be the best strategy to control the epithelial-mesenchymal transition (EMT) and increase patient survival because the research depicts that hyaluronidase has a role in maintaining the proliferation, invasion and migration of cancer cells. To the best of our knowledge and understanding, this is the first time we have described the chemopreventive potential of narirutin in PC-3 cells and its effect on hyaluronidase activity, a diagnostic marker in prostate carcinoma.

Therefore, this study investigates the anti-proliferative potential of narirutin in hormone-refractory prostate cancer cells (PC-3) by utilizing cell viability assays. Furthermore, the growth inhibitory potential was established by examining cell cycle phases. In addition, the efficacy of narirutin for enzyme inhibition was investigated in cell-free and cell-based assay systems. The qRT-PCR analysis was performed to confirm the expression level of hyaluronidase. Furthermore, *in silico* docking and molecular dynamic simulation investigations were conducted to corroborate *in vitro* data. This helped to detect docked pose and interacting amino acid residues, confirming a significant molecular interaction between narirutin and hyaluronidase.

2. Materials & methods

2.1. Materials

The solvents and chemicals used in the present study were of analytical grade. Phosphate buffer, sodium phosphate, sodium chloride, albumin bovine, sodium acetate, neutral red dye, hyaluronic acid, NAC, MTT, DCFDA dye, propidium iodide, SRB dye and narirutin (≥98%) purchased from Sigma-Aldrich Ltd. Banglore, India. DMSO, formaldehyde and isopropanol were procured from Merck Ltd., Mumbai, India. FBS, DMEM and RPMI were obtained from Gibco, Thermo Fischer Scientific, Mumbai, India. Sodium bicarbonate and TCA were purchased from Himedia, Mumbai, India. The prostate carcinoma (PC-3) and embryonic kidney (HEK-293) cells were acquired from NCCS, Pune, India.

2.2. Cell viability assays

The viability of PC-3 cells was assessed by SRB, NRU and MTT assay. The cultured PC-3 cells were seeded in 96-well plates overnight and treated with different concentrations of narirutin (0.001–100 μM) for 24h. The non-treated cells (control) were considered 100% viable, and treated cells were compared to control cells, as reported earlier (Singh et al., 2020).

The procedure of Mosmann (1983) was used to perform the MTT assay. The dye (0.5 mg/mL) was added to each well after 24h treatment with narirutin and further incubated for 4h at 37 °C in the dark. After that, the media of each well is replaced with DMSO (100 μL) and shaken to dissolve the crystals completely. The insoluble formazan crystals were solubilised in DMSO and gave a purple color. The color change was detected by measuring formazan concentration reflected in optical density measured at 570 nm. The method of Skehan et al. (1990) with minor modification was employed to perform the SRB assay. 100 μL of TCA (20%) was added for 1h at 4 °C, and the wells were washed four

times with tap water and then air dried at room temperature. When the wells were dried, 100 μL of dye (0.25% in 1% acetic acid) was added, and the plate was incubated for 30 min, followed by washing with acetic acid (1%) at least thrice, and then Tris-base (10 mM) was added to each well. The orbital shaker solubilises the bound dye and the absorbance was recorded at 515 nm.

Babich and Borenfreund (1991) reported method was utilized to carry out the NRU assay. The dye (50 μg/mL) was added to the treated and non-treated cells and incubated for 3h. After incubation, the media was removed, followed by adding calcium chloride (0.5%) and formaldehyde (0.5%) to fix the cells. Then, a dissolving solution containing ethanol (50%) and acetic acid (1%) was then added to the wells and incubated for 10 min. After that, the plate was shaken well, and the absorbance was recorded at 540 nm.

2.3. Cell cycle analysis

The experiment was done by following the protocol of Pathak et al. (2020). PC-3 cells were treated with narirutin at 10 μM and 100 μM followed by incubation for 24h. After incubation, the cells were collected by trypsinization followed by washing with PBS. Then, cells were fixed with 70% alcohol added dropwise, followed by vortexing. The fixed cells were washed twice with PBS, followed by a DNA extraction buffer added for 5 min. Afterwards, the buffer was removed, and PI (50 μg/mL) with RNAse A (200 μg/mL) was added to the cells and incubated in the dark for 30 min. After incubation, the stained cells were examined using an LSR II BD Biosciences flow cytometer. The findings represent the percent population obtained in different cell cycle phases, as reported earlier (Pathak et al., 2021).

2.4. ROS estimation

The effect on levels of intracellular ROS was examined using DCFH-DA staining as per the reported procedure of Pathak et al. (2020). PC-3 cells were treated with various concentrations of narirutin (10 μM and 100 μM) for 24h. Then, cells were harvested and washed with PBS, followed by incubation with DCFH-DA dye (10 μM) for 30 min in the dark. The amount of intracellular ROS generation is directly related to an increase or reduction in H2DCF fluorescence in cells. The effect was analysed using BD-FACS LSR II, and the acquisition was performed using FACS Diva software. The results were represented in terms of mean FITC obtained after 10,000 events, as reported earlier (Pathak et al., 2021).

2.5. Cell lysate preparation

The PC-3 cells were treated with narirutin in a concentration-dependent manner (0.1–100 μM) for 24h. After that, RIPA buffer was used to lyse the cells, and the protein was quantified by nanodrop. For the cell-free assay, the pure enzyme was used. For the cell-based assay, 10 μg of crude protein was used to perform the target inhibitory potential of narirutin.

2.5.1. Hyaluronidase assay

The experiment was done according to the method reported by Dorfman and Ott (1948). Dorfman and Ott first established the assay method in 1948. We have modified this method to evaluate a decrease in turbidity at 600 nm using spectrophotometry after combining hyaluronic acid and serum albumin at 37 °C using acidic pH. The experiments were performed in two different sets. One set contains different concentrations of narirutin (0.1–100 μM) incubated at 37 °C for 10 min in enzyme diluent buffer containing sodium phosphate (20 mM), sodium chloride (77 mM), bovine albumin (0.01%), and 4U/mL enzyme solution added to it. Another set contains diluent enzyme buffer alone. In the cell-based assay, the cell lysate was incubated with diluent enzyme buffer at 37 °C for 10 min. After incubation, the hyaluronic acid (0.3%) was added to the mixture and further incubated at 37 °C for 45 min in a cell-free and cell-based assay. Then, the diluent buffer was added to the mixture with a 5-fold volume for 10 min at room temperature, and the absorbance was recorded at 600 nm. The specific enzyme activity was calculated as described by Dorfman and Ott (1948), and then percent inhibition was calculated concerning control, as reported earlier (Fatima et al., 2021).

2.6. Real-time expression assay

PC-3 cells were treated with narirutin at 100 μM for 24h; the RNA was isolated using a trizol reagent. Primers were designed using Primer Express® Software v3.0 of the target gene sequence taken from NCBI (http://www.ncbi.nlm.nih.gov/) of human origin and synthesised from IDT (Integrated DNA Technology). The primer sequences of HYAL were as follows: forward primer TGGGCCCCTATGTGATCAAT, reverse primer ATGGCACCGCTGGTGACT. The forward and reverse sequences of GAPDH were CCACCCATGGCAAATTCC and TGGGATTTCCATTGATCACAAG, respectively. The cDNA kit (applied biosystems) was used to synthesise the cDNA. The syber green PCR master mix was used to perform the reaction in a thermal cycler programmed as 94 °C for 3 min for initial denaturation, 35 cycles of 94 °C for 1 min, 55 °C for 30 s, and 72 °C for 1 min. After 35 cycles of completion, the final extension was provided at 72 °C for 10 min. Then, the reaction was incubated at 4 °C for storage. The reaction mixture contained 0.5 μL forward primer, 0.5 μL reverse primer, 5 μL syber green, 0.2 μL ROX dye, 2 μL template cDNA, and 1.8 μL deionised water to make up to 10 μL/well in 384-well plate format. As previously reported, relative gene expression was computed for treated and non-treated (control) samples using GAPDH as an internal control for normalisation (Fatima et al., 2021).

2.7. In silico docking analysis

The interaction of narirutin with cyclin D1 (2W98), CDK-4 (6P8G), CDK-6 (1XO2), and hyaluronidase (2PE4) was examined by utilising the methodology of Trott et al. (2010) using Autodock vina. The 3D structure of narirutin was obtained from PubChem (Pubchem ID: 42431) in SDF format and then converted into PDB using Openbabel software. Likewise, the 3D structure of targeted proteins, including cyclin D1 (2W98), CDK-4 (6P8G), CDK-6 (1XO2), and hyaluronidase (2PE4), were obtained from the protein data bank. The proteins were filtered for hydrogen bonds, water molecules and missing atoms. At the same time, the ligand files were prepared in PDB after the energy minimisation. Ten runs were performed using a search algorithm. The UCSF chimera observed the binding analysis (interaction with amino acids) and the orientation. Ligplot was used to examine the hydrogen bonds and hydrophobic interaction, as reported earlier (Singh et al., 2021).

2.8. MD simulations

The molecular dynamic (MD) simulation was performed using GROMACS-2018.4 software at the central computational facility (CCF) of the Indian Institute of Information Technology, Allahabad, Prayagraj, Uttar Pradesh, India. The docked complex of hyaluronidase and NAC (PDB ID: 2PE4-Pubchem ID: 21115830), hyaluronidase and narirutin (PDB ID: 2PE4-Pubchem ID: 442431) were used, and the complexes were simulated using Charmm36 force field as reported earlier (Maurya et al., 2020). The protein topology files were generated using the TIP3P model, and ligand topology was created using the SwissParam web server (Zoete et al., 2011). The SPC water model was used to create the aqueous environment, and the system was neutralised by using Na+and Cl^- ions. The steepest descent algorithm, 1000 kJ mol^{-1} $nm^{-1,}$ was used to minimise the energy by selecting 50000 interactions for each system. Then, restrained the ligand, and the system was equilibrated with 310 K temperature and 1 bar pressure for 2 fs. The electrostatic interactions were calculated using the Particle Mesh Ewald method, and the Berendsen temperature coupling method was used to regulate the

temperature. The heavy atoms restraint conditions were positioned using LINCS constraints algorithms and a non-bonded pair list. After that, the MD run was performed for 60 ns, and after the termination of MD, the trajectories were used to observe the structural deviations by analysing the radius of gyration, root mean square deviation, root mean square fluctuations, Coulomb-Short Rang (Coul-SR) energy, Lennard Jones Short Range (LJ-SR) energy, solvent accessible surface area (SASA) energy, Hydrogen-bond, and principal component analysis (PCA) analysis.

2.9. MM/PBSA analysis

The binding free energy between the protein and ligands (NAC and NAR) complex was calculated using the MM/PBSA (Molecular Mechanic/Poisson–Boltzmann surface area) by the apolar and polar solvation potential energy calculations in the vacuum parameter. The MM/PBSA program was used to determine the sum of all the estimated energies to predict the binding energy between the protein and its ligands. The energies are generated every 1000 ps (Kumari et al., 2014). Further, the contribution energy of amino acid against the binding energy and interaction energies were calculated using the MM-PBSA method.

2.10. ADMET assessment

The absorption, distribution, metabolism, elimination and toxicity (ADMET) profiling of narirutin was done using online web servers Iazar and ADMETlab.

2.11. Statistical analysis

Data were calculated in Microsoft Excel (2007) and represented as mean ± SD. Table curve (2D windows version 4.07) was used to calculate the IC_{50}. Dunnett's test (one-way ANOVA) was employed to investigate the statistical significance.

3. Results

3.1. Narirutin reduced the viability of prostate carcinoma cells

The concentration-dependent effect of narirutin was examined in PC-3 cells by employing SRB NRU and MTT assays. The findings suggest that narirutin reduced more than 50% proliferation in MTT and SRB assays with IC_{50} values of 66.87 ± 10.87 μM and 59.80 ± 4.58 μM, respectively, while in NRU assay, it reduced the viability up to 32.67 ± 3.95% (Fig. 1). The viability of HEK-293 (normal cells) after narirutin treatment was 86.25 ± 2.44%, 80.33 ± 3.08%, and 78.50 ± 4.00% at 100 μM in MTT, SRB and NRU assay, respectively (Fig. 1) indicating a non-significant reduction in the viability of normal cell line. Podophyllotoxin (PDT) showed a growth reduction of 70.20 ± 2.70%, 64.82 ± 1.17% and 74.46 ± 7.02% in MTT, NRU and SRB assay, respectively. Since narirutin slows the proliferation of prostate cancer cells, further mechanistic analysis, including cell cycle, ROS estimation, and hyaluronidase activity was performed.

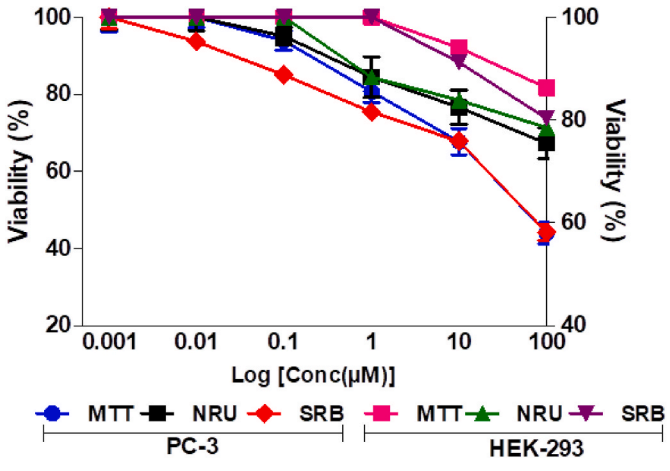

Fig. 1. Effect of narirutin on cell viability
The concentration-dependent (100–0.001 μM) effect of narirutin was observed in prostate carcinoma (PC-3) and human embryonic kidney (HEK-293) cells using MTT, NRU and SRB assay. Data represent the mean ± SD (n = 3).

3.2. Narirutin arrests the G0/G1 phase in prostate carcinoma cells

Narirutin reduced the viability of prostate cancer cells; therefore, cell cycle analysis was performed to corroborate whether the anti-proliferative effect of narirutin was mediated by arresting the cell cycle phases. Treatment with narirutin at 10 μM and 100 μM for 24h significantly modulate the cell cycle phases (Fig. 2A). The G0/G1 phase populations increased to 1.09 fold and 1.12 fold after treatment with narirutin at the tested concentrations. At both tested concentrations, a simultaneous reduction in S-phase and G2/M populations was also observed with narirutin. Narirutin arrest the G0/G1 phase; hence, its binding interaction with the cyclin-dependent kinase-4, 6 and cyclin D1 were examined. The docking analysis indicates that narirutin strongly interacted with CDK-4, CDK-6 and cyclin-D1 with the binding energy of -7.8 kcal/mol, -9.5 kcal/mol, and -8.7 kcal/mol. The docked binding poses are presented in Fig. 2B–D. Narirutin forms the hydrogen bond with the targeted proteins, suggesting the stability of the receptor-ligand complex.

3.3. Narirutin increased the reactive oxygen species generation in prostate carcinoma cells

The high levels of ROS are documented to reverse the chemotherapeutic resistance and induce cytotoxicity in tumorigenic cells. The evidence suggests that ROS elevation is the core mechanism of conventional cancer therapies and is directly associated with the death of cancer cells (Aggarwal et al., 2019). Therefore, narirutin mediated effect on ROS was analysed using DCFDA staining at 10 μM and 100 μM. Fig. 3A and B depicts that narirutin significantly increased the ROS production by 1.34 fold at higher tested concentration; however, at 10 μM, a non-significant reduction was observed. The finding indicates that narirutin acts as a pro-oxidant at higher concentrations.

3.4. Narirutin inhibit the activity of hyaluronidase

The enzyme activity of narirutin was assessed in both cell-free and cell-based test systems. In a cell-free assay, narirutin showed more than 70% enzyme activity inhibition at 100 μM, while a cell-based assay showed 56.35 ± 1.38% inhibition at 100 μM (Fig. 4A). The IC_{50} values are 11.17 ± 2.59 μM and 67.23 ± 6.42 μM in cell-free and cell-based assays, respectively. Further, the efficacy of narirutin was analysed at the transcript (mRNA) level of HYAL in PC-3 cells. The results are presented as Log relative quantification (Log RQ, Fig. 4B) and fold change concerning control. The findings indicate that narirutin down-regulates the expression of HYAL-1 non-significantly with the fold change of 1.24.

3.5. Narirutin showed stable and robust interaction with hyaluronidase

Narirutin inhibits hyaluronidase activity; thus, further *in silico* studies were conducted to determine whether the inhibitory potential of narirutin is mediated through the direct interaction with protein. The molecular interaction study indicates that narirutin showed binding energy of -7.67 kcal/mol and an inhibition constant of 2.40 μM (Table 1). The docked pose of narirutin with hyaluronidase is depicted in Fig. 4C and D. Ligplot studies showed that narirutin forms H-bonds with A chain of HYAL. Narirutin interacted with ASP129 and TYR247, which

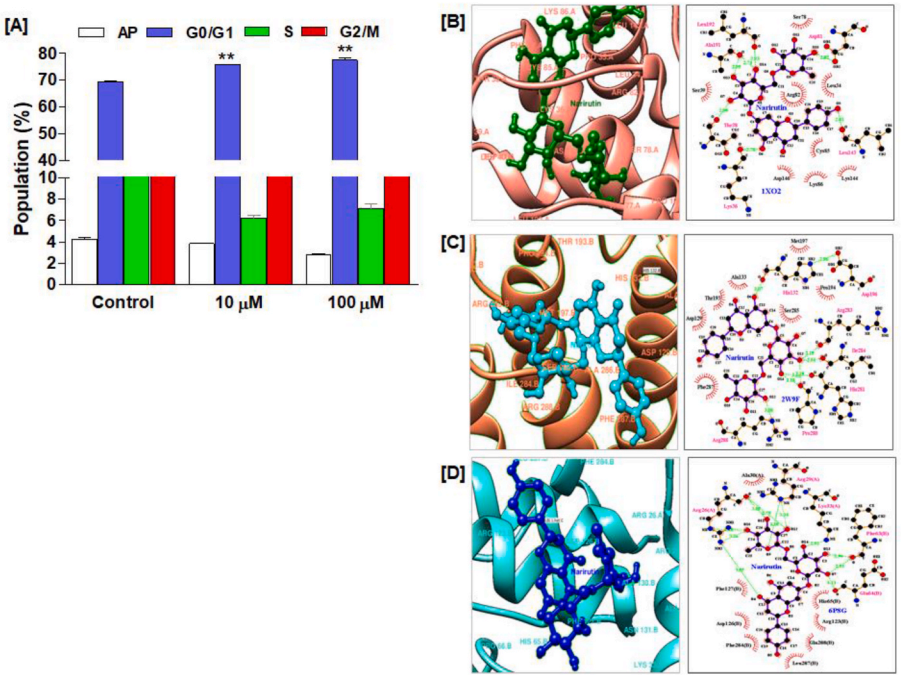

Fig. 2. Effect of narirutin on cell cycle phases of prostate carcinoma
The effect of narirutin at 10 μM and 100 μM was observed in prostate carcinoma (PC-3) cells. [A] Percent population observed in narirutin-treated and non-treated cells. [B] The docked poses of narirutin with cyclin-dependent kinase-6. [C] The docked poses of narirutin with cyclin D1 were obtained from ligplot and UCSF chimera. [D] The docked poses of narirutin with cyclin-dependent kinase-4. Data represent mean ± SD (n = 3). Dunnett's post hoc test was applied to observe the difference compared to non-treated cells. **p < 0.05 consider significant.

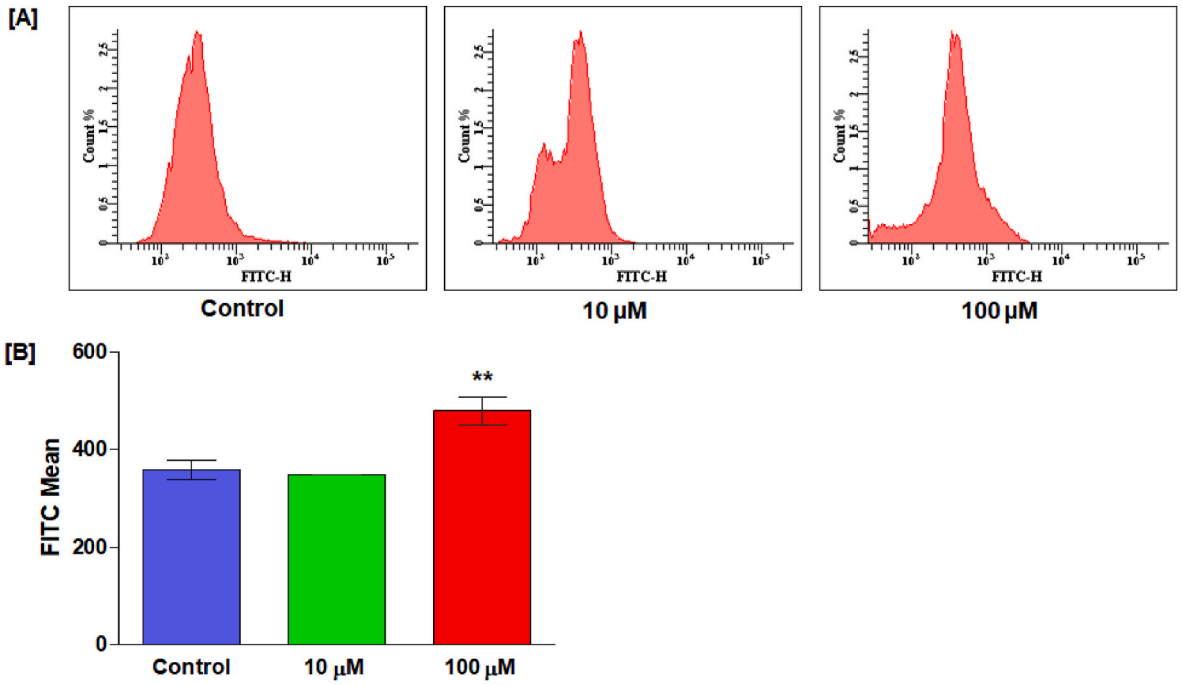

Fig. 3. Effect of narirutin on ROS levels of prostate carcinoma
The effect of narirutin on ROS levels at 10 μM and 100 μM was observed in prostate carcinoma (PC-3). [A] Histograms represents the changes in ROS levels. [B] FITC mean observed by DCFDA staining using Flow cytometry. Data represent mean ± SD (n = 3). Dunnett's post hoc test was applied to observe the difference compared to non-treated cells. **p < 0.05 consider significant.

are required to stabilise catalytic nucleophiles. Narirutin also interacts with GLU131, which acts as a proton donor for the hydroxyl leaving group and forms a hydrogen bond with SER245, ARG265, LYS144, GLU131 and TYR247. The *in silico* docking study findings were further confirmed by observing hyaluronidase's structural and conformational changes after ligation with NAR and NAC using Molecular Dynamic simulation on Gromacs 18.4.

The MD simulation of protein (Apo), NAC (Standard) and NAR complexes was performed for 60 ns. The RMSD graph in Fig. 5A and B suggests protein was comparatively highly unstable with a 2.76 nm average RMSD. In contrast, a complex protein with NAR (0.89 nm) and NAC (0.37 nm) were more stable and had no significant fluctuation in the structure. The RMSF of proteins and protein-ligand complexes fluctuated more during simulation than the protein individually. The average RMSF values of protein, complexes of protein-NAC and protein-NAR were 0.087 nm, 0.123 nm, and 0.147 nm, respectively. These

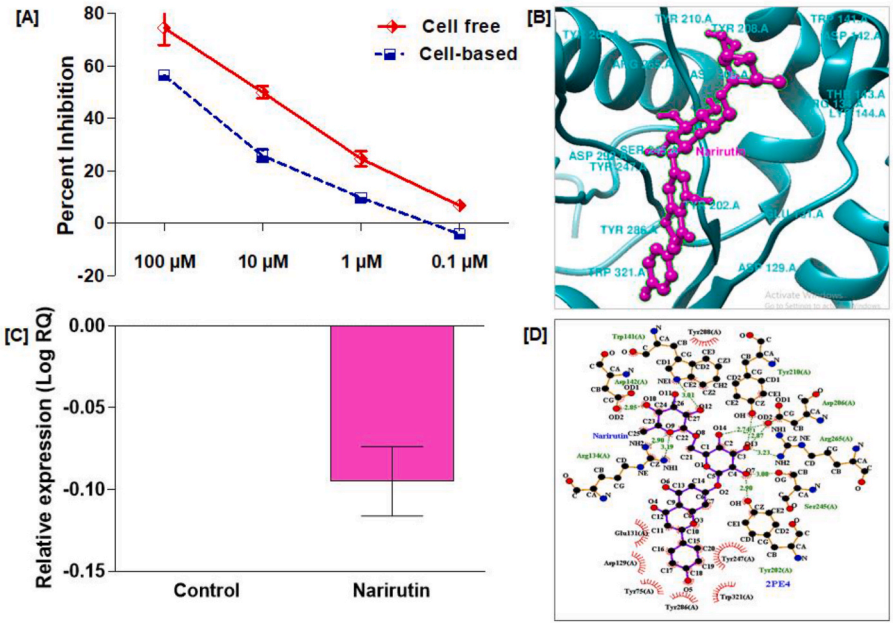

Fig. 4. Narirutin inhibits the activity of hyaluronidase in cell-free and cell-based test systems
The concentration-dependent effect of narirutin was observed in cell-free and cell-based test systems. [A] The percent inhibition of narirutin at different concentrations in cell-free and prostate carcinoma cells. [B] Effect of narirutin on m-RNA regulation of hyaluronidase in prostate carcinoma cells. [C] The docked poses of narirutin with hyaluronidase were obtained from the UCSF chimera. [D] The docked poses of narirutin with hyaluronidase representing hydrophobic interaction and H-bonds obtained from Ligplot. Data represent mean ± SD (n = 3). Dunnett's post hoc test was applied to observe the difference compared to non-treated cells. **p < 0.05 consider significant.

Table 1
Binding interaction of narirutin with the targeted receptors.

Targets	B E (kcal/mol)	Ki (mM)	H-bond length (Å)	H-bond residues	Hydrophobic residues	Residues within the region of 5 Å radius
Cyclin D1 (2W9F)	-8.7	4.14876E-07	3.07 3.19 2.94 3.19 3.20 3.18 3.08	HIS132 ARG283 ILE284 PHE280 HIS281 PHE280 ARG288	ASP129, THR193, ALA133, MET197, PRO194, SER285, PHE287	CYS135.B, THR193.B, HIS132.B, ALA133.B, ASP129.B, ALA286.B, PHE287.B, GLN291.B, ARG288.B, ILE284.B, SER285.B, MET197.B, ARG283.B, PRO194.B, PRO280.B, HIS281.B, LYS282.B
CDK-4 (6P8G)	-7.8	1.89729E-06	3.08 2.79 2.80 3.26 3.05 3.34 3.10 2.92 2.96 2.81 3.13	ARG26 ARG26 ARG26 ARG26 ARG26 ARG29 ARG29 LYS33 PHE63 PHE63 GLU64	ALA30, HIS65, ARG123, GLN288, LEU287, PHE284, ASP126, PHE127	ASP25.A, ARG26.A, ARG29.A, VAL27.A, ALA30.A, ALA130.B, ASN131.B, LYS33.A, PHE63.B, GLU64.B, PRO66.B, HIS65.B, PHE127.B, ARG126B, ASP126.B, LEU287.B, PHE284.B, GLN288.B
CDK-6 (1XO2)	-9.5	1.07414E-07	2.82 2.81 2.78 2.98 2.95 2.74 2.93	ASP81 LEU143 LYS36 THR38 ALA191 ALA191 LEU192	SER78, LEU34, ARG82, CYS85, LYS144, LYS86, ASP146, SER39	ARG66.B, LYS144.A, ASP146.A, LEU143.A, LYS86.A, PRO35.A, LEU34.A, ARG82.A, CYS85.A, PHE37.A, THR38.A, LYS36.A, VAL150.A, SER78.A, ASP81.A, SER39.A, TRP41.A, LEU40.A, ARG52.A, ALA191.A, LEU192.A, LEU185.A, LEU193.A, ILE198.A, PRO195.A, ALA152.A, PRO74.A, VAL150.A, VAL77.A, SER78.A, PRO35.A, LEU34.A, ARG82.A
Hyaluronidase (2PE4)	-9.6	9.072E-08	3.01 2.85 2.90 3.19 2.90 3.08 3.23 2.87 2.74 2.71	TRP141 ASP142 ARG134 ARG134 TYR202 SER245 ARG265 ASP206 ASP206 TYR210	TYR208, GLU131, ASP129, TYR75, TYR286, TRP321, TYR247	TYR262A, ARG265.A, ASP206.A, TYR210.A, TYR208.A, TRP141.A, ASP142.A, THR143.A, LYS144.A, ARG134.A, GLU131.A, ASP129.A, TRP321.A, TYR286.A, TYR202A, TYR247.A, SER245A, ASP292.A

BE: Binding energy; Ki: Inhibition constant; H-bond: Hydrogen bond.

results showed that protein obtains flexibility due to the ligation of NAC and NAR, significantly affecting the overall binding of the amino acid residues with the ligand atom (Fig. 5C and D). The Rg of protein was almost constant (2.268 nm) throughout simulation time, and ligated protein with NAC (2.308 nm) showed more fluctuation than NAR (2.281 nm; Fig. 5E and F). The graph of interaction energy reveals that

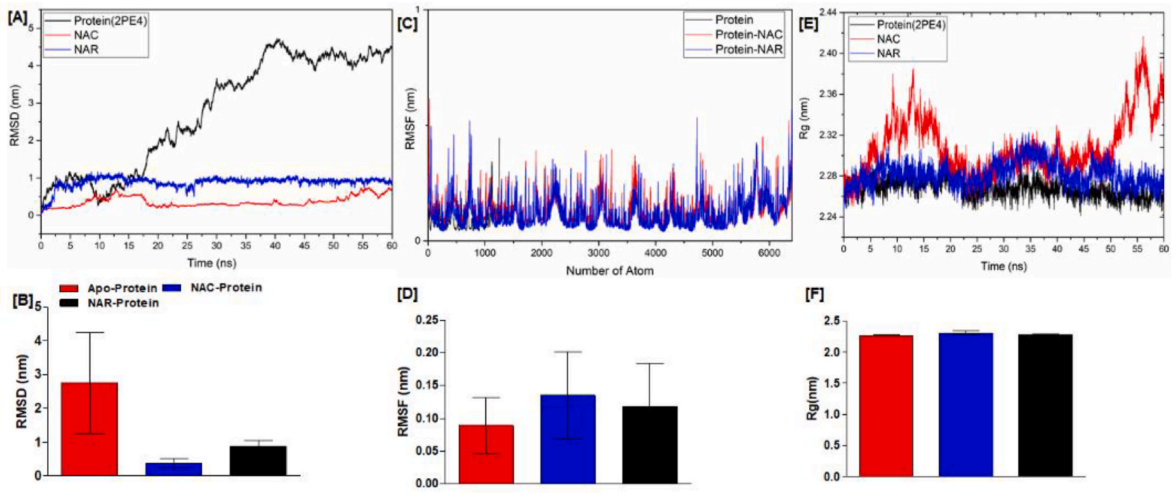

Fig. 5. Molecular dynamics simulation graphs observed using GROMACS
[A] Represents RMSD change observed during simulation. [B] Indicates average RMSD of Apo-protein, NAC (N-acetyl-L-cysteine), and NAR (Narirutin). [C] Represents root mean square fluctuation (RMSF) observed during simulation. [D] Indicates average RMSD of Apo-protein, NAC (N-acetyl-L-cysteine), and NAR (Narirutin). [E] Represents RMSD change observed during simulation. [F] Indicates average RMSD of Apo-protein, NAC (N-acetyl-L-cysteine), and NAR (Narirutin).

NAR shows more stable interaction while NAC shows fluctuation for both columbic-SR and LJ-SR interactions (Fig. 6A–D). The proteins' average energy per amino acid residue contribution over 60 ns during the simulation time against the binding affinity between the ligand molecules and the protein is depicted as the amino acid residues decomposition plot. The result of MMPSBA analysis revealed that the residue of amino acids identified to be participating in the interactions during the docking studies shows better stability and plays an essential role in the inhibitory activity of protein responsible for cancer cell proliferation and metastasis (Fig. 6E). NAR interacted and formed more hydrogen bonds with the protein NAC (Fig. 7A). The solvent-accessible surface area (SASA) of non-ligated and ligated proteins was calculated to analyse the changes in the hydrophilic and hydrophobic residues during the simulation. The SASA results showed that the ligated protein with NAC and NAR showed a somewhat higher SASA value than the unligated protein (Fig. 7B). The essential dynamic study used motion data during simulations to support the MD results. The data were obtained using principal component analysis (PCA) analysis. The most important associated eigenvalues throughout the dynamics of proteins are thought to be in the subspace around the eigenvectors. Using a covariance matrix created from the fluctuations in atomic location, the overall flexibility of the ligated and unligated proteins was examined (Maurya et al., 2020). The eigen vectors' plot showed that the protein with ligand showed less motion from the centre of the unligated protein, confirming the ligation's stability at 300 K (Fig. 7C).

3.6. *Narirutin does not act as a CYPs inhibitor and is non-toxic*

The physico-chemical properties indicate a high solubility of narirutin and high CaCO-2 permeability. It does not act as an inhibitor or substrate of p-gp. It did not cross the blood-brain barrier but showed plasma protein binding. It does not inhibit the different cytochromes (CYPs) and thus does not affect the metabolism. The predicted half-life of narirutin is 1.775 h, and the clearance rate is 0.578 mL/min/kg (Table 2). Narirutin did not reveal hepatotoxicity, skin sensitisation, carcinogenicity, and mutagenesis, but the lethal toxicity dose was high

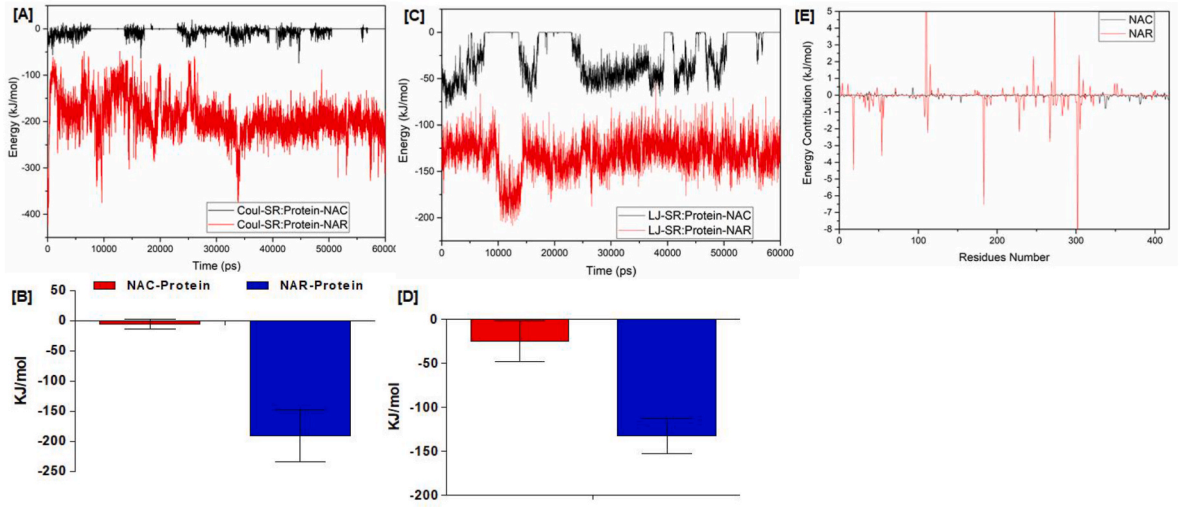

Fig. 6. Interaction energy graphs observed during MD simulation
[A] Represents Coulombic-Sort Range energy analysed during 60 ns simulation. [B] Indicates average of Coul-SR energy of Apo-protein, NAC and protein, NAR and protein. [C] Represents Lennard-Jones sort Range energy analysed during 60 ns simulation. [D] Indicates the average LJ-SR energy of Apo-protein, NAC and protein, NAR and protein. [E] The residue decomposition plot of the interactions between the protein and the ligands (NAC & NAR).

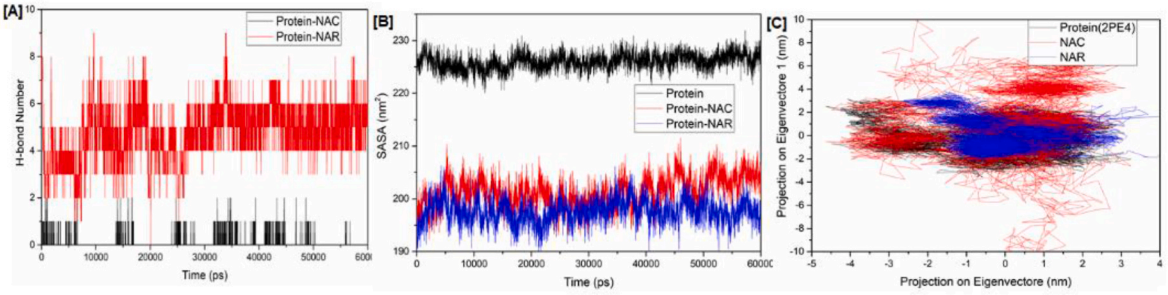

Fig. 7. Structural and interaction graphs generated during molecular dynamics
[A] H-bond formation between protein-NAC and protein-NAR complexes. [B] Solvent-accessible surface area (SASA) analyzed in apo-protein, NAC and protein, NAR and protein. [C] Projection of the motion of the protein in the phase space along the first two principal eigenvectors at 300 K: protein Apo (black) vs ligated protein (NAC and NAR).

Table 2
ADMET properties of narirutin.

Physiochemical properties	
Log S (Solubility)	−3.001 log mol/L
Log D7.4 (Distribution coefficient D)	0.932
Log P	−1.165
Absorption	
Caco-2 permeability	−6.645 cm/s
P gp-inhibitor	NO
P gp-substrate	NO
Distribution	
Plasma protein binding	76.284%
Volume distribution	−0.917L/Kg
Blood-brain Barrier	NO
Metabolism	
CYP1A2 inhibitor	NO
CYP3A4 inhibitor	NO
CYP2C9 inhibitor	NO
CYP2C19 inhibitor	NO
CYP2D6 inhibitor	NO
Elimination	
$T_{1/2}$ (half-life time)	1.775 h
Clearance rate	0.578 mL/min/kg
Toxicity	
Human hepatotoxicity	NO
Carcinogenicity (Mouse)	NO
Carcinogenicity (Rat)	NO
Carcinogenicity (Rodent)	NO
Mutagenesis	NO
Skin sensitisation	NO
LD_{50} of acute toxicity	360.439 mg/kg
Maximum recommended daily dose (Human)	23.4 mg/kg bw/day

LD_{50}, Lethal dose; CYP, Cytochrome p450; P-gp, P-glycoprotein; $T_{1/2}$, Time required for plasma concentration of a drug to decrease by 50%.

(Table 2).

4. Discussion

Prostate cancer is commonly diagnosed in males and is the second leading cause of mortality among men. Most patients experience hormone-refractory (androgen-independent) cancer, which resists advanced clinical therapy and increases mortality, probably due to p53 mutations, increasing DNA instability, androgen receptor mutations, and changes in gene expression., It is a type of prostate cancer that cannot be managed by hormone therapy. The treatment options for refractory hormone malignancies include supportive care, second-line hormonal adjustments, and cytotoxic therapy. The chemotherapeutic agents increased the palliative benefits and response rate but did not improve survival (Martel et al., 2003; Sonpavde et al., 2006; Hou et al., 2016). Hence, the efforts must be focused on identifying the investigational agents with a novel mechanism of action and having low toxicity on normal cells. Therefore, the chemopreventive potential of narirutin, a dietary flavanone, was examined in PC-3 cells by performing cell viability assays. Fig. 1 demonstrates that narirutin potentially reduced the viability of PC-3 cells in a concentration-dependent manner while not being effective against HEK-293 (human embryonic kidney cell line). Besides, findings indicate that narirutin-induced reduction in the cell viability of PC-3 cells was not mediated by altering the integrity of lysosomes. An earlier report by Shammugasamy et al. (2019) supported our finding that indicates narirutin-containing peel extract of *C. sinensis* L. suppressed the proliferation of prostate cancer cells (LNCaP and PC-3).

The cell cycle is an essential biological phenomenon regulated by proteins, and the deregulation leads to cancer progression. The cell cycle is divided into G0/G1, S, G2, and M phases, and any change or arrest by chemical interventions reduces the proliferation of cancer cells (Schwartz and Shah, 2005). Fig. 2 depicts that narirutin induced G0/G1 phase arrest in PC-3 cells and suppressed their multiplication by arresting them into the resting phase. Besides, narirutin showed strong binding interaction and formed a hydrogen bond with the cyclin D1, CDK-4 and CDK-6. This could be a strong indicator that narirutin binds to the appropriate cyclins and CDKs and undergoes conformational changes that result in the inhibition of specific proteins, arresting the cells in the resting phase.

Reactive oxygen species are a significant regulator of diverse signalling pathways in cancer cells. The evidence reveals that ROS increase is the primary mechanism of traditional cancer therapy and is closely related to the death of cancer cells (Aggarwal et al., 2019). Hence, the effect of narirutin in ROS generation was explored using DCF-DA staining. Fig. 3 indicates that narirutin increased ROS generation compared to the non-treated cells. Anthracyclins and doxorubicin-induced ROS generation are widely used to treat bladder cancer, breast cancer, acute lymphocytic leukaemia, and Kaposi's sarcoma (Aggarwal et al., 2019; Pilco-Ferreto and Calaf, 2016; Panchuk et al., 2017). The findings suggest that ROS induction might be a possible mechanism for narirutin-mediated growth inhibition of PC-3 cells.

Karl Meyer first introduced the hyaluronidase term to indicate enzymes that degrade HA. HYAL is considered a prognostic and diagnostic biomarker in tumor cells. Prostate cancer five-year survival was reduced, and clinical recurrence was predicted by HYAL-1 and hyaluronic acid overexpression (Gomez et al., 2009). Prostate cancer cells that express HYAL-1 produce a considerable amount of HA fragments when injected in mice intra-prostatically and are found to be more metastatic (≈90% of lymph node metastasis) abrogated by knockdown of HA synthesis in aggressively metastatic prostate cancer cells (McCarthy, 2005; Patel et al., 2002). The up-regulation of HYAL-1 expression at the mRNA level has been reported in many cancer types, particularly bladder and prostate cancer, where its expression is down-regulated in alternative splice variants (Chao et al., 2007). Fig. 4 demonstrates that narirutin strongly interacts with hyaluronidase and

the critical amino acid residues involved in catalytic stabilisation. Besides, it inhibits hyaluronidase activity in cell-free and cell-based test systems (Fig. 4A).

Moreover, the expression analysis confirmed the narirutin-mediated downregulation of hyaluronidase in PC-3 cells (Fig. 4B). It has been observed that fisetin treatment significantly decreased hyaluronidase's protein and mRNA expression in prostate cancer cells (Lall et al., 2016). Naringenin and 7-O-butyl naringenin showed uncompetitive inhibition against hyaluronidase (Moon et al., 2009). Flavonoid glycosides were determined as hyaluronidase inhibitors, especially 7-O-glucuronides and aglycones, including kaempferol and quercetin (Kubínová et al., 2019). The RMSD of protein and protein-ligand complexes were calculated, and the graph was plotted to analyse the stability of the complex. To analyse the dynamic stability of protein-ligand complex structure, RMSD is a universal measure of structural fluctuation. To understand the effects of ligands on the protein structure flexibility and stability, the mean per residue fluctuation of the ligand-protein complex and protein backbone were calculated using RMSF analysis. The radius of gyration (Rg) analysis reveals the structure compatibility, folding of protein structure, and mass-weighted mean square distance of atoms from their centre mass (Maurya et al., 2020). Fig. 5 depicts that the folding and compactness of protein complexes with NAC changes more than the NAR complex.

Furthermore, the strength of thunderation of ligands with protein, Short-range coulombic and Lennard-jones potential energy was also estimated. The non-bonded interaction energy between ligands and proteins was calculated in these interactions. The results indicate that NAR binding interaction was more stable than NAC (Fig. 6). The interaction potential between the protein and ligands was calculated by analysing hydrogen bonding throughout the simulation time. Fig. 7 revealed that NAR forms more hydrogen bonds than NAC, suggesting NAR forms a more stable complex than NAC. The modification of hyaluronic acid (HA) was done by hyaluronidase into low molecular weight fragments that will interact with CD44 membrane receptors. Because hyaluronidase was overexpressed in cancer cells, a high and low-weight HA fragment abundance was seen. Upon binding, HA activates the pathways (RAS-MAP kinase and PI3K) that are involved in cancer cell proliferation, motility, chemo-resistance, survival and invasion. The extracellular domain of CD44 has an HA-binding part that makes it a more specific ligand (Chen et al., 2018). To suppress the activation of tumor-promoting pathways, cancer therapy must modify the interaction of HA and CD44 or the levels of HA in the extracellular matrix. Narirutin inhibits hyaluronidase's activity and forms a stable complex with it. Thus, it might change the binding with HA and disrupts the formation of low molecular weight HA synthesis. Due to the unavailability of low molecular weight HA fragments, it could not interact with CD44 receptors and thus might suppress the activation of downstream pathways. Besides, CD44 contributes to lowering ROS levels by glutamate-cystine transporter xCT, thereby maintaining the ROS level in cancer cells. This process helps cancer cells in ROS defence and tumor progression and makes cancer cells resistant to chemo and radiotherapy (Yusupov et al., 2021; Cowman, 2017). Narirutin acts as a pro-oxidant and increases ROS levels by altering the mitochondrial function or enhancing endoplasmic reticulum stress (ER). The excess generation of ROS (hydroxyl radicals) causes the ring to open and cleave the glycosidic linkage of HA. This modification leads to the disruption in the interaction of CD44 and HA, thereby hindering the signalling pathways involved in the progression and survival of cancer cells (Fig. 8). Narirutin did not show hepatotoxicity, carcinogenicity, and skin sensitisation. Besides, it did not cross the BBB and act as a CYPs inhibitor. The present study suggests the potential of narirutin for prostate cancer prevention. These findings also advocate for medicinal chemistry interventions to enhance the efficacy of narirutin. Although, a few limitations remain to be addressed, including Western blot analysis to validate the target modulatory potential of narirutin and the interaction of the downstream pathway of CD44 and HA along with the effect on mitochondrial potential and xenograft model experiments.

5. Conclusion

Narirutin potentially reduced the viability of hormone-refractory prostate cells and induced G0/G1 phase arrest. Besides, it inhibits the activity of hyaluronidase, a diagnosis marker in prostate carcinoma. Further, MD analysis confirmed that narirutin maintains the compactness of hyaluronidase and forms a stable complex; thus might be responsible for inhibiting hyaluronidase. Moreover, it induced ROS generation in PC-3 cells that might lead to the oxidation of HA fragments and hinder the interaction with CD44 receptors, thereby suppressing the signalling pathways associated with the proliferation and survival of prostate carcinoma cells. Additionally, it did not depict skin sensitisation, carcinogenicity, mutagenesis or hepatotoxicity. Narirutin possess potent chemopreventive efficacy and thus could be used to synthesise novel analogues with improved efficacy. However, further experimental validations are required to establish its effectiveness.

Funding

CSIR-CIMAP DU2/MLP-11.

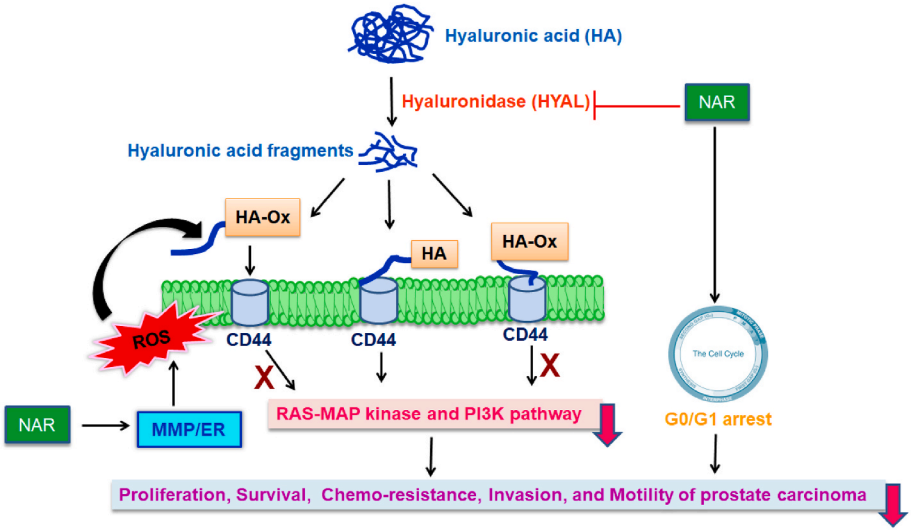

Fig. 8. Possible chemopreventive mechanism of narirutin
The black color arrow represents the sequence of signalling while the pink color shows the down-regulation of pathway HA: Hyaluronic acid; MMP: Mitochondrial membrane potential; ER: Endoplasmic reticulum; ROS: Reactive oxygen species; NAR: Narirutin; MAPK: Mitogen-activated protein kinase; PI3K: Phosphoinositide 3-kinases; Ras: Rat sarcoma virus kinase. (For interpretation of the references to color in this figure legend, the reader is referred to the Web version of this article.)

Conflict of interest

None.

CRediT authorship contribution statement

Shilpi Singh: did experiments. **Akhilesh Kumar Maurya:** did experiments. **Abha Meena:** Formal analysis, did in silico experiment planning, analysis and manuscript writing. **Nidhi Mishra:** did analysis of MD simulations work. **Suaib Luqman:** Formal analysis, did cell line based experiment planning, analysis and manuscript writing.

Declaration of competing interest

The authors declare that they have no known competing financial interests or personal relationships that could have appeared to influence the work reported in this paper.

Data availability

The data related with research work is included within manuscript in form of figure and table

Acknowledgement

We are obliged to the Director, CSIR-Central Institute of Medicinal and Aromatic Plants, Lucknow, for the research facilities. SS is grateful to CSIR for her fellowship.

References

Aggarwal, V., Tuli, H.S., Varol, A., Thakral, F., Yerer, M.B., Sak, K., Varol, M., Jain, A., Khan, M., Sethi, G., 2019. Role of reactive oxygen species in cancer progression: molecular mechanisms and recent advancements. Biomolecules 9, 735.
Babich, H., Borenfreund, E., 1991. Cytotoxicity of T-2 toxin and its metabolites determined with the neutral red cell viability assay. Appl. Environ. Microbiol. 57, 2101–2103.
Bahall, M., 2017. Prevalence, patterns, and perceived value of complementary and alternative medicine among cancer patients: a cross-sectional, descriptive study. BMC Compl. Alternative Med. 17, 1–9.
Chakraborty, S., Basu, S., 2017. Multi-functional activities of citrus flavonoid narirutin in Alzheimer's disease therapeutics: an integrated screening approach and in vitro validation. Int. J. Biol. Macromol. 103, 733–743.
Chao, K.L., Muthukumar, L., Herzberg, O., 2007. Structure of human hyaluronidase-1, a hyaluronan hydrolysing enzyme involved in tumor growth and angiogenesis. Biochemistry 46, 6911–6920.
Chen, L., Li, T., Wang, Y.L., Dong, Y., Zhuang, S.X., Wang, D.F., Yang, W.P., 2015. Simultaneous determination and quantitation of anthraquinones, lignans and flavonoids in Xiao-Cheng-Qi tang, Hou-Po-san-Wu tang and Hou-Po-Da-Huang tang by HPLC. Yao Xue Xue Bao= Acta Pharmaceutica Sinica 50, 887–892.
Chen, C., Zhao, S., Karnad, A., Freeman, J.W., 2018. The biology and role of CD44 in cancer progression: therapeutic implications. J. Hematol. Oncol. 11, 1–23.
Cheng, W.-L., Huang, C.-Y., Tai, C.-J., Chang, Y.-J., Hung, C.-S., 2018. Maspin enhances the anticancer activity of curcumin in hormone-refractory prostate cancer cells. Anticancer Res. 38, 863–870.
Cherrak, S.A., Merzouk, H., Mokhtari-Soulimane, N., 2020. Potential bioactive glycosylated flavonoids as SARS-CoV-2 main protease inhibitors: a molecular docking and simulation studies. PLoS One 15 (10), e0240653.
Chun-yan, F.U., Hui-yu, W., Yong-hui, L.I.U., Yang, W., 2020. Simultaneous determination of eight components in Xuefu Zhuyu Decoction based on UPLC-ESI-IT-TOF-MS method. Nat. Prod. Res. Dev. 32, 1006.
Cowman, M.K., 2017. Hyaluronan and hyaluronan fragments. Adv. Carbohydr. Chem. Biochem. 74, 1–59.
Dorfman, A., Ott, M.L., 1948. A turbidimetric method for the assay of hyaluronidase. J. Biol. Chem. 172, 367–375.
Drozdoff, L., Klein, E., Kiechle, M., Paepke, D., 2018. Use of biologically-based complementary medicine in breast and gynecological cancer patients during systemic therapy. BMC Compl. Alternative Med. 18, 1–7.
Fatima, K., Masood, N., Wani, Z.A., Meena, A., Luqman, S., 2021. Neomenthol prevents the proliferation of skin cancer cells by restraining tubulin polymerisation and hyaluronidase activity. J. Adv. Res. 34, 93–107.
Fontana, F., Raimondi, M., Marzagalli, M., Di Domizio, A., Limonta, P., 2020. Natural compounds in prostate cancer prevention and treatment: mechanisms of action and molecular targets. Cells 9, 460.
Fu, C., Xia, Z., Liu, Y., Lu, H., Zhang, Z., Wang, Y., Fan, X., 2016. Qualitative analysis of major constituents from Xue Fu Zhu Yu Decoction using ultra high performance liquid chromatography with hybrid ion trap time-of-flight mass spectrometry. J. Separ. Sci. 39, 3457–3468.
Gomez, C.S., Gomez, P., Knapp, J., Jorda, M., Soloway, M.S., Lokeshwar, V.B., 2009. Hyaluronic acid and HYAL-1 in prostate biopsy specimens: predictors of biochemical recurrence. J. Urol. 182, 1350–1356.
He, Y., Cheng, P., Wang, W., Yan, S., Tang, Q., Liu, D., Xie, H., 2018. Rapid investigation and screening of bioactive components in simo decoction via LC-Q-TOF-MS and UF-HPLC-MD methods. Molecules 23, 1792.
He, Y.-J., Zhu, M., Zhou, Y., Zhao, K.-H., Zhou, J.-L., Qi, Z.-H., Zhu, Y.-Y., Wang, Z.-J., Xie, T.-Z., Tang, Q., 2020. Comparative investigation of phytochemicals among ten citrus herbs by ultra high performance liquid chromatography coupled with electrospray ionisation quadrupole time-of-flight mass spectrometry and evaluation of their antioxidant properties. J. Separ. Sci. 43, 3349–3358.
Hou, R., Wang, Y., Xu, Y., Zheng, Y., Ma, M., Hu, B., 2016. Theranostic hollow/mesoporous organosilica nanospheres enhance the therapeutic efficacy of anticancer drugs in metastatic hormone-resistant prostate cancer. RSC Adv. 6, 94058–94067.
Josefsson, A., Adamo, H., Hammarsten, P., Granfors, T., Stattin, P., Egevad, L., Laurent, A.E., Wikström, P., Bergh, A., 2011. Prostate cancer increases hyaluronan in surrounding nonmalignant stroma, and this response is associated with tumor growth and an unfavorable outcome. Am. J. Pathol. 179, 1961–1968.
Kallifatidis, G., Hoy, J.J., Lokeshwar, B.L., 2016. Bioactive natural products for chemoprevention and treatment of castration-resistant prostate cancer. In: Seminars in Cancer Biology. Elsevier, pp. 160–169.
Kubínová, R., Gazdová, M., Hanáková, Z., Jurkaninová, S., Dall'Acqua, S., Cvačka, J., Humpa, O., 2019. New diterpenoid glucoside and flavonoids from Plectranthus scutellarioides (L.) R. Br. South Afr. J. Bot. 120, 286–290.
Kumari, R., Kumar, R., Consortium, O.S.D.D., Lynn, A., 2014. g_mmpbsa A GROMACS tool for high-throughput MM-PBSA calculations. J. Chem. Inf. Model. 54, 1951–1962.
Lall, R.K., Syed, D.N., Khan, M.I., Adhami, V.M., Gong, Y., Lucey, J.A., Mukhtar, H., 2016. Dietary flavonoid fisetin increases abundance of high-molecular-mass hyaluronan conferring resistance to prostate oncogenesis. Carcinogenesis 37, 918–928.
Li, C.-H., Wang, L., Kuo, C.-H., Chen, Y.-T., Tsai, M.-L., Hung, C.-H., 2020. Narirutin suppresses M1-related chemokine interferon-gamma-inducible protein-10 production in monocyte-derived M1 cells via epigenetic regulation. Phcog. Mag. 16, 479.
Lokeshwar, V.B., Lokeshwar, B.L., Pham, H.T., Block, N.L., 1996. Association of elevated levels of hyaluronidase, a matrix-degrading enzyme, with prostate cancer progression. Cancer Res. 56, 651–657.
Lokeshwar, V.B., Rubinowicz, D., Schroeder, G.L., Forgacs, E., Minna, J.D., Block, N.L., Nadji, M., Lokeshwar, B.L., 2001. Stromal and epithelial expression of tumor markers hyaluronic acid and HYAL1 hyaluronidase in prostate cancer. J. Biol. Chem. 276, 11922–11932.
Martel, C.L., Gumerlock, P.H., Meyers, F.J., Lara Jr., P.N., 2003. Current strategies in the management of hormone refractory prostate cancer. Cancer Treat Rev. 29, 171–187.
Maurya, A.K., Mulpuru, V., Mishra, N., 2020. Discovery of novel coumarin analogs against the α-glucosidase protein target of diabetes mellitus: pharmacophore-based QSAR, docking, and molecular dynamics simulation studies. ACS Omega 5, 32234–32249.
McCarthy, J.B., 2005. Hyaluronan Biosynthesis in Prostate Cancer. MINNESOTA UNIV MINNEAPOLIS.
Moon, S.-H., Kim, K.-T., Lee, N.-K., Han, Y.-S., Nah, S.-Y., Cho, S.-G., Park, Y.-S., Paik, H.-D., 2009. Inhibitory effects of naringenin and its novel derivatives on hyaluronidase. Food Sci. Biotechnol. 18, 267–270.
Mosmann, T., 1983. Rapid colorimetric assay for cellular growth and survival: application to proliferation and cytotoxicity assays. J. Immunol. Methods 65, 55–63.
Ngo, S.T., Quynh Anh Pham, N., Thi Le, L., Pham, D.-H., Vu, V.V., 2020. Computational determination of potential inhibitors of SARS-CoV-2 main protease. J. Chem. Inf. Model. 60, 5771–5780.
Panchuk, R.R., Skorokhyd, N.R., Kozak, Y.S., Lehka, L.V., Moiseenok, A.G., Stoika, R.S., 2017. Tissue-protective activity of selenomethionine and D-panthetine in B16 melanoma-bearing mice under doxorubicin treatment is not connected with their ROS scavenging potential. Croat. Med. J. 58, 171.
Patel, S., Turner, P.R., Stubberfield, C., Barry, E., Rohlff, C.R., Stamps, A., Tyson, K., Terrett, J., Box, G., Eccles, S., 2002. Hyaluronidase gene profiling and role of HYAL-1 overexpression in an orthotopic model of prostate cancer. Int. J. Cancer 97, 416–424.
Patel, P., Barve, K., Bhatt, L.K., 2020. Narirutin-rich fraction from grape fruit peel protects against transient cerebral ischemia reperfusion injury in rats. Nutr. Neurosci. 1–11.
Pathak, G., Singh, S., Kumari, P., Hussain, Y., Raza, W., Luqman, S., Meena, A., 2020. Cirsilineol inhibits proliferation of lung squamous cell carcinoma by inducing ROS mediated apoptosis. Food Chem. Toxicol. 143, 111550.
Pathak, G., Singh, S., Kumari, P., Raza, W., Hussain, Y., Meena, A., 2021. Cirsimaritin, a lung squamous carcinoma cells (NCIH-520) proliferation inhibitor. J. Biomol. Struct. Dyn. 39, 3312–3323.
Pilco-Ferreto, N., Calaf, G.M., 2016. Influence of doxorubicin on apoptosis and oxidative stress in breast cancer cell lines. Int. J. Oncol. 49, 753–762.
Rawla, P., 2019. Epidemiology of prostate cancer. World J. Oncol. 10, 63.
Schwartz, G.K., Shah, M.A., 2005. Targeting the cell cycle: a new approach to cancer therapy. J. Clin. Oncol. 23, 9408–9421.
Seo, C.-S., Shin, H.-K., 2020. Quality assessment of traditional herbal formula, Hyeonggaeyeongyo-tang through simultaneous determination of twenty marker components by HPLC–PDA and LC–MS/MS. Saudi Pharmaceut. J. 28, 427–439.

Shammugasamy, B., Valtchev, P., Dong, Q., Dehghani, F., 2019. Effect of citrus peel extracts on the cellular quiescence of prostate cancer cells. Food Funct. 10, 3727–3737.
Singh, S., Kumari, P., Hussain, Y., Luqman, S., Meena, A., Kanaojia, D., 2020. Isothymusin, a potential inhibitor of cancer cell proliferation: an in silico and in vitro investigation. Curr. Top. Med. Chem. 20, 1898–1909.
Singh, S., Meena, A., Luqman, S., Meena, A., 2021. Acacetin and pinostrobin as a promising inhibitor of cancer-associated protein kinases. Food Chem. Toxicol. 151, 112091.
Skarmoutsos, I., Skarmoutsos, A., Katafigiotis, I., Tataki, E., Giagini, A., Adamakis, I., Alamanis, C., Duvdevani, M., Sitaras, N., Constantinides, C., 2018. Hyaluronic acid and hyaluronidase as possible novel urine biomarkers for the diagnosis of prostate cancer. Med. Oncol. 35, 1–6.
Skehan, P., Storeng, R., Scudiero, D., Monks, A., McMahon, J., Vistica, D., Warren, J.T., Bokesch, H., Kenney, S., Boyd, M.R., 1990. New colorimetric cytotoxicity assay for anticancer-drug screening, JNCI. J. Natl. Cancer Inst. 82, 1107–1112.
Sonpavde, G., Hutson, T.E., Berry, W.R., 2006. Hormone refractory prostate cancer: management and advances. Cancer Treat Rev. 32, 90–100.
Toygar, I., Yeşilbalkan, Ö.U., Kürkütlü, M., Aslan, A., 2020. Complementary and alternative medicines used by cancer patients to cope with chemotherapy-induced constipation. Compl. Ther. Clin. Pract. 39, 101108.
Trott, O., Olson, A.J., 2010. AutoDock Vina: Improving the speed and accuracy of docking with a new scoring function, efficient optimisation, and multithreading. J. Comput. Chem. 31, 455–461.
Tsujimoto, T., Yoshitomi, T., Maruyama, T., Yamamoto, Y., Hakamatsuka, T., Uchiyama, N., 2019. High-resolution liquid chromatography–mass spectrometry-based metabolomic discrimination of citrus-type crude drugs and comparison with nuclear magnetic resonance spectroscopy-based metabolomics. J. Nat. Prod. 82, 2116–2123.
Yu, J.-W., Deng, K.-Y., Peng, T., Zhu, B.-Y., Liu, H.-Y., 2013. Simultaneous determination of six ingredients in Huoxiang Zhengqi oral liquid by UPLC. Zhongguo Zhong Yao Za Zhi= Zhongguo Zhongyao Zazhi= China Journal of Chinese Materia Medica 38, 2314–2317.
Yusupov, M., Privat-Maldonado, A., Cordeiro, R.M., Verswyvel, H., Shaw, P., Razzokov, J., Smits, E., Bogaerts, A., 2021. Oxidative damage to hyaluronan–CD44 interactions as an underlying mechanism of action of oxidative stress-inducing cancer therapy. Redox Biol. 43, 101968.
Zhang, H.-J., Cheng, Y.-Y., 2006. An HPLC/MS method for identifying major constituents in the hypocholesterolemic extracts of Chinese medicine formula 'Xue-Fu-Zhu-Yu decoction. Biomed. Chromatogr. 20, 821–826.
Zhang, B., Qi, D., Deng, X., Ma, Z., Wu, Y., Xue, Z., Kebebe, D., Lu, P., Pi, J., Guo, P., 2019. Quantification of nineteen bioactive components in the ancient classical Chinese medicine formula of Wen-Dan decoction and its commercial preparations by UHPLC-QQQ-MS/MS. Molecules 24, 2031.
Zoete, V., Cuendet, M.A., Grosdidier, A., Michielin, O., 2011. SwissParam: a fast force field generation tool for small organic molecules. J. Comput. Chem. 32, 2359–2368.
Zuniga, K.B., Zhao, S., Kenfield, S.A., Cedars, B., Cowan, J.E., Van Blarigan, E.L., Broering, J.M., Carroll, P.R., Chan, J.M., 2019. Trends in complementary and alternative medicine use among patients with prostate cancer. J. Urol. 202, 689–695.